Published in final edited form as:
J Neurosci Methods. 2007 August 15; 164(1): 75–85.

Electrophysiological and pharmacological validation of vagal afferent fiber type of neurons enzymatically isolated from rat nodose ganglia

Bai-Yan Li[a,b] and **John H Schild**[a,*]

a *Dept. of Biomedical Engineering, Indiana University Purdue University Indianapolis, Indianapolis, Indiana 46202*

b *Dept. of Pharmacology, Harbin Medical University, Harbin, 150081, CHINA*

Abstract

An unavoidable consequence of enzymatic dispersion of sensory neurons from intact ganglia is loss of the axon and thus the ability to classify afferent fiber type based upon conduction velocity (CV). An intact rat nodose ganglion preparation was used to randomly sample neurons (n = 76) using the patch clamp technique. Reliable electrophysiological and chemophysiological correlates of afferent fiber type were established for use with isolated neuron preparations. Myelinated afferents (~25%) formed two groups exhibiting strikingly different functional profiles. One group (n = 10) exhibited CVs in excess of 10 m/s and narrow (< 1 ms) action potentials (APs) while the other (n = 9) had CVs as low as 4 m/s and broad (> 2 ms) APs that closely approximated those identified as unmyelinated afferents (n = 57) with CVs less than 1 m/s. A cluster analysis of select measures from the AP waveforms strongly correlated with CV, producing three statistically unique populations ($p < 0.05$). These groupings aligned with our earlier hypothesis (Jin et al., 2004) that a differential sensitivity to the selective purinergic and vanilloid receptor agonists can be used as reliable pharmacological indicators of vagal afferent fiber type. These metrics were further validated using an even larger population of isolated (n = 240) nodose neurons. Collectively, these indicators of afferent fiber type can be used to provide valuable insight concerning the relavence of isolated cellular observations to integrated afferent function of visceral organ systems.

Keywords

Sensory neuron; visceral afferent; fiber conduction velocity; tissue slice; action potential; whole-cell patch; capsaicin; αβ-m-ATP

INTRODUCTION

Neurons of the cranial and dorsal root ganglia have peripheral receptors that play an essential role in transducing and transmitting sensory information to the central nervous system. Neurons within these ganglia have long been used as a surrogate system for studying the ion channel basis for the voltage and chemical sensitivities of visceral and peripheral sensory receptors,

*Corresponding author Address: 723 W. Michigan St., Suite SL174, Indianapolis, IN 46202, E-mail: jschild@iupui.edu (J.H. Schild). Phone: 317-274-9747.

which are quite small, delicate and generally inaccessible for direct study. These neurons are often enzymatically isolated from the ganglia and prepared for *in vitro* experimental study where pharmacological challenges and cell properties such as transmembrane potential can be reliably controlled and integrated cellular responses can be precisely measured. The field of sensory neuron electrophysiology, as an example, has dramatically advanced our appreciation for the potential role of voltage- and ligand-gated ion channels in pathophysiologies such as visceral and somatic pain.(Wood and Docherty, 1997;Waxman, 2001; Sugiura, Dang et al., 2005) Unfortunately, enzymatic dispersion of the ganglia separates the neuron soma from its axonal projections. As a result, during the course of an experiment investigators are left to infer afferent fiber type (i.e. myelinated or unmyelinated) based upon such indirect measures as somatic action potential waveshape, sensitivity to select ion channel antagonists or even cell size. (Gallego and Eyzaguirre, 1978; Schild, Clark et al., 1994;Schild and Kunze, 1997;Lancaster and Weinreich, 2001;Huang and Hanani, 2005;Yoshida and Matsumoto, 2005) However, substantial evidence exists in the literature suggesting that such indirect measures of nerve function and extent of myelination are an oversimplification.(Belmonte and Gallego, 1983;Stansfeld and Wallis, 1985;Harper and Lawson, 1985a;Harper and Lawson, 1985b; Lee, Chung et al., 1986;Villiere and McLachlan, 1996; Cabanes, Lopez et al., 2002)

To address this technical shortcoming we developed an intact ganglion slice preparation that makes possible patch clamp study of neurons with intact afferent fibers.(Li and Schild, 2002) Here, each cell under study can be reliably classified as a myelinated or an unmyelinated afferent based upon the conduction velocity (CV) of the afferent axon. This measure, in turn, can be used to estimate fiber diameter and extent of myelination, thereby further classifying the anatomical characteristics of the sensory neuron understudy.(Lee, Chung et al., 1986) This method has proved to be highly reliable for current clamp investigation of somatic action potential discharge characteristics from nodose neurons of identified afferent fiber type. However, precise biophysical study of the pharmacological, voltage- and time-dependent properties of the transmembrane ionic channels that are essential for neuronal excitability is markedly impeded by the restricted access to the cell bodies and the presence of intact axons. As a result it is extremely difficult to maintain precise control over transmembrane potential of the cell body when using intact preparations and thus the quality of voltage clamp recording protocols are severely limited. Here, we endeavored to both identify and validate a set of correlative measures of action potential waveshape and pharmacological sensitivities that can reliably predict afferent fiber type from sensory neurons isolated from the nodose ganglia.

Through a comparative analysis of data recorded from nodose neurons with intact afferent fibers and data recorded from neurons enzymatically isolated from the nodose ganglion we demonstrate that select measures of somatic action potential waveshape characteristics can collectively be used as a reliable indicator of afferent fiber type. Furthermore, we show that isolated nodose neurons exhibiting broad somatic action potential waveforms with a prominent hump or delay in repolarization can not be assumed to have originated from cell bodies with unmyelinated afferent fibers. This latter observation has significant implications concerning the widely recognized heterogeneity in action potential discharge properties and chemical sensitivities of isolated vagal afferent neurons of presumably unmyelinated afferent origin.

MATERIALS AND METHODS

Use of all animals adhered to protocols approved by the Institutional Animal Care and Use Committee of the Purdue School of Science at IUPUI.

Preparation of intact ganglia

Slices of nodose ganglia with intact vagal axons were prepared in a manner previously described.(Li and Schild, 2002) Briefly, Sprague-Dawley (Harlan, Indianapolis) adult rats

(200–250g) of either gender were used for the slice preparation. The unrestrained rats were placed in an airtight induction chamber for inhalation of the anesthetic Metofane (Methoxyflurane, Schering-Plough Animal Health Corp NJ). Upon lack of reflex response to tail pinch the animals were immediately sectioned at the mid-auxiliary region, preserving at least 2 cm of the vagus nerve. The nodose ganglia with attached vagus were excised under stereomicroscopy (x40). The tissue was immediately placed in chilled (4°C) recording solution. Slicing exposed the interior of the ganglion capsule and the tissue was placed in a solution of Earle's balance salt solution (Sigma, MO) containing type II Collagenase (1.0 mg/ml) at 37 ° C for 40 – 45 min followed by the solution containing Trypsin-3X (5 mg/ml) for another 20 – 22 min. The tissue was moved to the bath perfusion chamber and allowed to recover for one hour prior to recording.

Preparation of neonatal isolated neurons

Cell bodies from the nodose ganglia were prepared in a manner previously described [Schild et al, 1994; Li and Schild, 2002a] Briefly, the nodose ganglia from Sprague-Dawley (Harlan, Indianapolis) neonatal rats pups (3–9 days postpartum) of either gender were surgically excised under stereomicroscopy (x40) and immediately placed into a chilled (4 – 8 °C) nodose complete medium (NCM) consisting of 90 ml of DME-F-12 medium (Sigma, St. Louis, MO), 5 ml of Fetal Bovine Serum (Hyclone, Logan UT), 1.0 ml of Penicillin-Streptomycin (Invitrogen, Grand Island, NY), and 100 μM of MITO + Serum Extender (Collaborative Res, Bedford MA). The ganglia were subsequently treated in a 37°C solution of Earle's balanced salt solution containing Trypsin-3X (5 mg/ml) for 30 min. The enzyme solution was then replaced with NCM and the ganglia titrated with an aspiration pipette to free the cell bodies for plating onto a Poly-D-Lysine (0.5 mg/ml aqueous solution) coated cover slip. The isolated nodose neurons were maintained in an incubation chamber (5% CO2 – 95% air) at 37°C for at least two but not more than eight hours prior to recording.

Preparation of adult isolated neurons

Surgical isolation of the adult rat (200–300g) nodose ganglia was performed under stereomicroscopy (x40) and immediately placed in chilled NCM. The ganglia were then enzymatically treated by the application of 10 Units/ml of Papain (Worthington, Lakewood, NJ) @ 37 °C for 20 min, followed by 1 mg/ml of type II Collagenase and 2.5 mg/ml of Dispase (Roche, USA) @ 37°C for a additional 30 min. All other details concerning mechanical dispersion, plating and incubating were the same as for the neonatal preparation.

Recording solutions and agonists

The extracellular and pipette recording solutions differed depending upon the experimental procedure. For recording of somatic action potential waveforms the extracellular solution consisted of (in mM): 137.0 NaCl, 5.4 KCl, 1.0 $MgCl_2$, 2.0 $CaCl_2$, 10.0 glucose, 10.0 *N*-2-hydroxyethylpiperazine-*N*′-2-ethanesulfonic acid (HEPES), and the pipette solution consisted of (in mM): 10.0 NaCl, 50.0 KCl, 50.0 K_2SO_4, 5.0 $MgCl_2$. For recording of whole cell Na^+ currents the extracellular solution contained (mM): 50.0 NaCl, 10.0 $MgCl_2$, 10.0 HEPES, 25.0 glucose and the pipette solution contained (mM); 7.0 NaF, 140.0 NMDG, 2.0 TEA-Cl, 2.0 $MgCl_2$, 10.0 HEPES. The pH for pipette solutions and bath solutions were adjusted to 7.25 and 7.35 using 1N Pipes/KOH and 1N NaOH. Osmolarity of the extracellular and intracellular solutions were adjusted to 310 – 315 and 290 – 295, respectively, using D-Manitol (Sigma, MO). Just prior to recording the pipette solution was adjusted to include 2.0 mM Mg-ATP, 2.0 mM Na-GTP along with 4.0 mM Bapta-K/Bapta-Na and 0.25 mM $CaCl_2$ for a final buffered $[Ca^{2+}]_i$ of 10 nM.

Two selective agonists of ligand gated ion channels were utilized on account of their demonstrated ability to discriminate between myelinated and unmyelinated afferents.(Jin,

Bailey et al., 2004) These agonists were prepared using the extracellular action potential recording solution and consisted of either 100 nM Capsaicin (CAP) or 10 μM αβ-methyl-ATP (αβ-m-ATP) both from Sigma-Aldrich Co (St. Louis, MO).

Electrophysiology

Patch recording electrodes (7052, Corning) were pulled (P-87, Sutter) and polished (MF-830, Narishige) down to a resistance of 1.2 – 1.8 MΩ. The whole-cell current clamp technique was used for recording of somatic action potentials and the voltage clamp technique for recording of whole cell Na^+ currents. Details concerning individual recording protocols are presented in the results. The experimental protocol, data acquisition, storage, display and preliminary analysis were carried out using p-CLAMP (V9.02) and a 200A Axopatch recording amplifier (Axon Instruments, CA). All experiments were conducted at room temperature.

Vagal afferents were stimulated using a bipolar Pt-IR electrode placed a measured distance from the recording electrode. Fiber conduction velocity (CV) was calculated by dividing this distance by the time delay between recording of the stimulus artifact and the somatic action potential. When using the slice preparation for voltage clamp recording(Li and Schild, 2002) CV could still be measured but in a slightly different manner. Since the pipette solution would not support the generation of an action potential CV was measured under a cell attached patch configuration, i.e. seal formation but without rupturing the cell membrane. Stimulating the vagus while bathing the tissue in the normal extracellular action potential solution resulted in a current transient recorded at the cell body that corresponded to the arrival at the soma of the fiber conducted action potential. The time delay between recording of the stimulus artifact and this current transient was used in calculating fiber CV. Following this measure, the extracellular solution was exchanged for that used in the voltage clamp recordings.

Data analysis and statistics

All data were analyzed using Clampfit software (Axon Instruments) with pooled statistics calculated using Excel. Data presented as mean ± SD with significance assessed using a two-way Student's t-test or ANOVA where appropriate.

RESULTS

The overarching objective of this study is to establish and validate two simple and convenient methods whereby neurons enzymatically isolated from the nodose sensory ganglia can be reliably classified as myelinated or unmyelinated afferent neurons. One method relies upon a strong correlation which exists between select measures of somatic action potential waveshape and afferent fiber conduction velocity. The other involves pharmacological classification of a neuron as a myelinated or an unmyelinated afferent based upon a differential sensitivity to the selective ligand channel agonists Capsaicin (CAP) and αβ-methyl-ATP (αβ-m-ATP). The certitude of these classification methods is derived from a large sample (n = 76) of patch clamp recordings from nodose neurons with intact axons where afferent fiber type can be classified as myelinated or unmyelinated based upon measure of axon conduction velocity (CV) at room temperatures.

Conduction velocity and action potential waveshape

Patch recording from 76 randomly selected nodose neurons with intact axons revealed three functionally distinct populations of cells based upon measures of CV and select features of corresponding somatic action potential wave shapes. (Figure 1 and Table 1) Thirteen percent (10/76) of the cells classified here as Atype myelinated afferents exhibited fiber CVs in excess of 10 ms (10 – 18 m/sec) with brief (< 1 ms) somatic action potential durations and upstroke and downstroke velocities well in excess of 300 V/s and −100 V/s, respectively. Twelve percent

(9/76) of the cells classified here as Ah-type myelinated afferents exhibited fiber CVs of at least 4 m/s but not more than 18 m/s with broad duration (> 1 ms) somatic action potential waveforms with upstroke velocities in excess of 200 V/s but rarely more than 300 V/s and downstroke velocities rarely more than −50 V/s. All Ah-type cells also exhibited a marked hump or delay over the repolarization phase of the somatic action potential waveform which accounted for the significantly broader action potential duration and slower downstroke velocity of these myelinated afferent neurons as compared with the A-type population of nodose neurons (Figure 1 and Table 1). Seventy five percent (57/76) of the cells exhibited fiber CVs that never exceeded 1 m/s at room temperatures and all exhibited broad duration (> 2 ms) somatic action potential waveforms with upstroke velocities that rarely exceeded 125 V/s and downstroke velocities that rarely exceeded −50 V/s. As with the population of Ah-type cells, all unmyelinated C-type afferent neurons exhibited a marked hump or delay over the repolarization phase of the somatic action potential waveform. (Figure 1 and Table 1) Such similarities in waveform characteristics of myelinated Ah-type and unmyelinated C-type afferent neurons underlies our hypothesis that the widely publicized heterogeneity in the pharmacological sensitivities and electrophysiological characteristics of presumably C-type nodose neurons may in fact be a consequence arising from differences in afferent fiber type (see Discussion).

Measure of CV in cell attached mode

For instances where the intact ganglion preparation can be used for voltage clamp study of ion channel biophysics (e.g. some outward K^+ currents, see (Li and Schild, 2002)), afferent classification would be a valuable adjunct to understanding the physiological role of particular ion channel subtypes in sensory neuron function. However, the requisite whole cell access and exchange of the intracellular ionic composition to one suitable for voltage clamp study would negatively impact conduction along the axon and eliminate the possibility of evoking a normal somatic action potential. This difficulty can be solved by bathing the intact ganglia in the action potential recording solution and patching onto the cell body for forming a gigaohm seal but not rupturing the membrane. In this manner, a nerve evoked action potential can conduct along the afferent axon. When arriving at the cell body the resulting transmembrane current can be detected at the patch recording electrode (Figure 1C–E) and the time delay between the stimulus artifact and the arrival of this waveform can be used to calculate fiber CV. The accuracy of this measurement technique was validated by comparing CV measures made using normal intracellular and extracellular action potential recording solutions before (i.e. cell attached) and after going whole cell. A comparison of the average CVs from each of the three groups revealed no statistical difference between CVs measured using a cell attached or whole cell patch recording configuration (i.e. 14.2 ± 0.9 m/s and 14.2 ± 1.1 m/s for myelinated A-type fibers, 10.5 ± 4.1 m/s and 10.5 ± 4.4 m/s for myelinated Ah-type fibers and 0.68 ± 0.10 m/s and 0.68 ± 0.14 m/s for unmyelinated C-type fibers.)

Cluster analysis

Select measures of somatic action potential waveshape from nodose neurons of identified afferent type based upon measure of CV and from isolated nodose neurons revealed at least three distinct features which showed marked statistical differences between the three functional groups of A-, Ah- and C-type afferent neurons, namely APFT, UV_{APD50}, and DV_{APD50}. (Table 1) Further examination of this observation using a clustering analysis technique similarly demonstrated three statistically different ($p < 0.05$) populations of afferent neurons. (Figure 3A) This analysis was applied to action potential waveforms recorded from a large population ($n = 240$) of isolated neonatal nodose neurons. These data showed a similar distribution of three statistically distinct ($P < 0.05$) populations of afferent neurons. The relative percentages of A-type (~12%, 29/240), and Ah-type (~11%, 27/240) myelinated afferent neurons and C-type (77%, 184/240) unmyelinated afferent neurons closely approximated those from the intact

ganglia preparation were afferent fiber type was conclusively identified according to measures of CV (Figure 3B and Table 1).

Another often used correlate of afferent fiber type especially in the dorsal root ganglion literature is cell diameter or the corresponding measure of whole cell capacitance (WCC). Interestingly, the measures of WCC of nodose neurons from both the intact adult and isolated neonatal preparations showed a continuous normal distribution with no statistically significant correlation with afferent fiber type as identified by CV or measures of action potential waveshape that can otherwise classify an isolated neuron as a myelinated or unmyelinated afferent. (Figure 3 and Table 1).

Pharmacological identification of afferent fiber type

In a previous study that incorporated the intact ganglia preparation we demonstrated that the fast conducting A-type myelinated nodose afferents were positively effected by the selective purinergic receptor (P2X) agonist αβ-m-ATP but unaffected by the selective vanilloid receptor (VR1) agonist CAP.(Jin, Bailey et al., 2004) Here, using a population of Ah-type myelinated afferents we test the hypothesis that a differential sensitivity to these two agonists can be a reliable indicator of afferent fiber type in both intact ganglion and isolated neuron preparations. In cells (n = 4) functionally identified as Ah-type based upon CV αβ-m-ATP (10 μM) evoked a large inward current with temporal dynamics typical of purinergic receptor activation while in this same cell CAP (100 nM) failed to evoke a transmembrane current response (Figure 4A). Sensitivity to these two agonists was tested in a subset (19 of 74) of isolated neonatal nodose neurons using a current clamp patch configuration. Here, isolated cells classified as A-type (n = 6) or Ah-type (n = 5) myelinated afferents based upon collective measures of APFT, UV_{APD50} and DV_{APD50} showed a positive response to 10 μM αβ-mATP but were unaffected by application of 100 nM CAP. (Figure 4B and 4C) In stark contrast those isolated cells classified as C-type (n = 8) based upon the same waveform measures were unaffected by 10 μM αβ-mATP where as 100 nM CAP evoked a prominent inward current with amplitude and temporal dynamics typical of VR1 receptor activation (Figure 4C). Subsequent analysis further verified that such a differential sensitivity to αβ-mATP and CAP can be a reliable indicator of afferent fiber type. Here, (Figure 4, lower panel) CAP-positive and αβ-mATP-negative isolated neurons clustered accord to measures that collectively identify unmyelinated C-type afferent neurons (compare w/Figure 3) while all cells exhibiting a positive response to αβ-m-ATP and a negative response to CAP clustered into two statistically distinct groups ($p < 0.05$) of A-type and Ah-type myelinated afferent neurons.

Implication of afferent identification in voltage-clamp study of isolated nodose neurons

The use of isolated cell preparations and voltage clamp protocols specifically designed for the study of select members of the superfamilies of Na^+, Ca^{+2} and K^+ ion channel subtypes makes possible high resolution biophysical study of ion channel dynamics under precise control of transmembrane voltage and chemical concentrations. For such investigations conclusive identification of afferent fiber type can serve as a power adjunct to interpreting the physiological significance of ion channel subtypes underlying the neuronal discharge characteristics of visceral sensory neurons of known afferent fiber type. We show here examples from isolated adult nodose neurons prepared for voltage clamp study of the tetrodotoxin-resistant $Na_v1.8$ ion channel subtype. Obviously the requisite chemical compositions for the extracellular media and the intracellular patch recording electrode eliminates the possibility for afferent classification based upon measures of somatic action potential waveshape. However, a differential sensitivity to the selective VR1 agonist CAP (100 nM) suggests that Ah-type nodose neurons with myelinated afferent fibers prominently express a tetrodotoxin-resistant $Na_v1.8$ whole cell current albeit with markedly different time and voltage characteristics as the $Na_v1.8$ whole cell current expressed in unmyelinated C-type

afferent neurons identified by sensitivity to CAP. (Figure 5) These findings are in contradiction to the longstanding assumption that myelinated nodose afferents express a singular class of tetrodotoxin-sensitive $Na_v1.7$ ion channels while only unmyelinated nodose afferents express the tetrodotoxin-resistant $Na_v1.8$ subtype.(Schild, Clark et al., 1994;Schild and Kunze, 1997) Further examination along these lines may reveal an as yet unappreciated physiological explanation for the broad heterogeneity in the voltage- and time-dependent characteristics of the tetrodotoxin-resistant $Na_v1.8$ channel current in presumed C-type nodose neurons as compared to the tetrodotoxin-sensitive $Na_v1.7$ channel current exclusively expressed in A-type myelinated afferent nodose neurons.

DISCUSSION

The reflexogenic consequences of selective activation of myelinated as compared with unmyelinated sensory afferent pathways in the cardiovascular, gastrointestinal and pulmonary systems as well as the etiology of selective afferent dysfunction in peripheral sensory neuropathies offer important insights into the neurophysiological foundations of human health and disease. (Fan and Andresen, 1998; Fan, Schild et al., 1999; Santiago, Ferrer et al., 2000; Kubin, Alheid et al., 2006; Blackshaw, Brookes et al., 2007) The field of cellular neuroscience is rapidly expanding our appreciation for the anatomical organization of sensory afferent subtypes and the selective expression of molecularly distinguishable proteins such as those of the superfamily of transmembrane transient receptor potential ion channels.(Hjerling-Leffler, Alqatari et al., 2007). Rigorous and well controlled *in vitro* study of such proteins is critical to advancing our understanding of integrated sensory neuron function. Patch clamp electrophysiology and the isolated cell preparation have greatly contributed to this effort. Recent advances in automated patch-clamping technologies offer high throughput capabilities for incorporation of this technique with other automated cell-based electrophysiological and biochemical assays.(Gorelik, Gu et al., 2002; Stett, Burkhardt et al., 2003; Wang and Li, 2003) Although this would strongly suggest an ever increasingly important role for isolated neuron preparations, the lack of a robust, reliable and real-time indicator of afferent fiber type markedly limits the potential for interpretations regarding integrated physiological function. The real-time classification methods demonstrated in this study will make the veritable classification of afferent fiber type possible for isolated preparations of vagal afferent neurons.

Evidence for three distinct populations of rat nodose sensory neurons

Patch recording from 76 randomly selected nodose neurons at room temperatures using an intact ganglion preparation revealed three functionally distinct types of sensory afferents (Figure 1). The A-type are presumed to be larger diameter myelinated afferents on account of fiber CVs always in excess of 10 m/s, brief duration (< 1 m/s) action potential waveforms and marked excitability in response to step depolarizing currents. The C-type are presumed to be smaller diameter unmyelinated afferents on account of fiber CVs always less than 1 m/s, broad duration (2–4 m/s) action potential waveforms with a prominent hump or delay over the time course of repolarization and a rather muted excitability in response to step depolarizing currents, ranging from short bursts to sustained low frequency repetitive discharge. A third group, Ah-type, exhibited CVs ranging from 4–18 m/s at room temperatures and therefore clearly myelinated afferents but with a somatic action potential waveshape that was more characteristic of the C-type population of unmyelinated afferents. Excitability in response to step depolarizing currents spanned the spectrum of discharge characteristics exhibited by the A-type and C-type afferents.

The most striking observation came about through a cluster analysis of select measures of action potential waveshape characteristics (Figure 2, Table 1). Here, measures of APFT, UV_{APD50}, and DV_{APD50} coalesced into three statistically distinct ($p < 0.05$) and

nonoverlapping populations, each precisely aligned according to afferent fiber type (Figure 3A). Plotting the same measures from a large population (n = 240) of isolated neonatal nodose neurons again clearly revealed three statistically distinct ($p < 0.05$) and nonoverlapping populations (Figure 3B). While strikingly similar to the relative groupings from neurons with known fiber CV further validation was required. Using the intact ganglion preparation and building upon an earlier observation concerning a differential sensitivity of vagal afferents to the selective P2X agonist αβ-m-ATP and the selective VR1 agonist CAP(Jin, Bailey et al., 2004) myelinated Ah-type afferents were exposed to both agonists, with only αβ-m-ATP effecting a response (Figure 4A). This differential sensitivity was also exhibited across a population of isolated neonatal nodose neurons (Figure 4B–C, bottom panel) again demonstrating that myelinated nodose afferent neurons are unaffected by CAP (100 nM) but respond with a prominent inward current in the presence of αβ-m-ATP (10 μM). As expected, unmyelinated nodose afferents exhibited an opposite pattern of agonist sensitivity.

Potential physiological significance of myelinated Ah-type afferents

The “Ah afferent phenotype”, i.e. a myelinated afferents with a somatic action potential exhibiting a hump or delay over the repolarization phase has been previously observed in sensory neurons of the rabbit nodose and mouse trigeminal ganglia.(Stansfeld and Wallis, 1985; Cabanes, Lopez et al., 2002) Our data show a distribution of myelinated A- and Ah-type and unmyelinated C-type afferents (~13%, 12% and ~75% respectively) in rat that is similar to these earlier studies. By and large the physiological significance of the Ah afferent phenotype remains unclear. Perhaps the most definitive evidence comes from studies of glossopharyngeal afferents in cat.(Belmonte and Gallego, 1983) Here, the authors show a subclass of chemoreceptor and baroreceptor neurons with myelinated axons and somatic action potentials with a hump over the time course of repolarization. For rat, it remains to be determined what functional role these Ah afferents serve in visceral sensory reception but intriguing possibilities can be found in studies of reflex control of arterial blood pressure.

Based upon physiological studies of reflex control of arterial blood pressure a postulate has been put forth that there are two functional types of arterial baroreceptor afferents and that each type contributes differently to the regulation of blood pressure.(Seagard, Hopp et al., 1993) The Type I baroreceptors are presumed to be faster conducting myelinated afferents and responsible for rapid dynamic control of baroreflex regulation. Type II baroreceptors are presumed to be both smaller diameter myelinated and unmyelinated C-fiber afferents with much less of an effect upon baroreflex sensitivity but a significant role in regulating tonic control of mean arterial pressure. These Type II baroreceptors have been shown to have a range of conduction velocities that aligns quite will with our CV measures across populations of myelinated Ah- and unmyelinated C-type afferents. It remains to be determined if there exists a subclass of Ah-type myelinated afferents that can be functionally identified as aortic baroreceptors.

Clearly, the Ah phenotype presents functional and ion channel characteristics that span the extremes typical of large myelinated A-type and unmyelinated C-type vagal afferents. For example, our voltage clamp data from isolated adult neurons pharmacologically classified as myelinated Ah-type and unmyelinated C-type clearly show evidence of a tetrodotoxin-resistant whole cell Na^+ current, presumably arising from the $Na_v1.8$ subtype of voltage-gate Na^+ ion channels. When used in conjunction with fiber dye labeling techniques that make possible fluorescent identification an isolated nodose neuron as a baroreceptor afferent, the real-time methods for afferent classification presented here offers tremendous potential to broaden our knowledge concerning the functional role of ion channel subtypes across integrated physiological function, bringing together observations from isolated *in vitro* cell preparations and *in situ* whole animal reflex studies that clearly demonstrate a differential role for myelinated

and unmyelinated afferents in reflex control of arterial blood pressure.(Seagard, Hopp et al., 1993;Fan and Andresen, 1998)

Significance of pharmacological identification of afferent type in isolated neuron preparations

Meaningful interpretations of the physiological significance of observations from isolated neuron preparations would benefit greatly from reliable identification of afferent fiber type. Neurochemical markers such as neurofilament cocktails, myelin basic protein, substance P, isolectin B4 and other antibodies have been successfully used to distinguish between myelinated and unmyelinated afferents but only in fixed tissue preparations.(Glazebrook, Schilling et al., 2005; Ruscheweyh, Forsthuber et al., 2007) Recent attempts at pharmacological classification during the course of *in vitro* cellular electrophysiological study have often involved selective agonists for P2X receptors, a family of ligand-gated ion channels responsive to ATP and CAP a selective agonist for the vanilloid receptor, a subtype of the superfamily of transient receptor (TRP) channel proteins (TRPV). While it is possible that some of these receptor subtypes may be segregated according to physiological function evidence exists in the DRG literature for expression of P2X and TRPV receptors across both myelinated and unmyelinated DRG afferents.(Dunn, Zhong et al., 2001;Clapham, 2003; Hjerling-Leffler, Alqatari et al., 2007) Indeed, the CAP sensitive vanilloid receptor (TRPV1) was recently shown to be prominently, but not exclusively, expressed in C-fiber DRG neurons. (Kobayashi, Fukuoka et al., 2005) And thus, at least for isolated sensory neurons preparations from the DRG a definitive method for real-time pharmacological classification remains elusive.

Bielefeldt (2000) and others have shown that upwards of 80% of nodose neurons express mRNA for the VR1 receptor, a percentage that closely approximates the prevalence of unmyelinated afferents in the nodose ganglia.(Mei, Condamin et al., 1980; Bielefeldt, 2000) And yet there have been reports that only 30–50% of isolated rat nodose neurons are functionally responsive to CAP (i.e. an agonist evoked transmembrane current).(Benson, Eckert et al., 1999;Bielefeldt, 2000). Further contradictions arise in studies of mouse nodose neurons with fiber CVs in the range of 0.7 and 1.5 m/s and therefore presumably unmyelinated afferents. These “faster” conducting afferents were insensitive to the effects of CAP but responsive to both ATP and the selective P2X receptor agonist αβ-m-ATP while fibers conducting below 0.7 m/s were responsive to both CAP and αβ-m-ATP.(Kollarik, Dinh et al., 2003) It is unknown if this reflects differences across species or that in mouse these faster conducting “C-fibers” may in fact be analogous to the lightly myelinated Ah-type afferents in rat nodose. Extension of the intact rat nodose ganglia preparation(Li and Schild, 2002) to a mouse model may reveal as yet unappreciated correlations between electrophysiological and pharmacological properties and afferent fiber type.

Still, our results strongly support the hypothesis from other studies that a differential sensitivity to P2X and VR1 receptor agonists can identify vagal afferent pathways as myelinated or unmyelinated, respectively. (Fan and Andresen, 1998; Bailey, Jin et al., 2002; Doyle, Bailey et al., 2002; Jin, Bailey et al., 2004) Furthermore, our new observations concerning the lack of sensitivity to CAP of myelinated Ah-type neurons may help to resolve some of the contradictory observations concerning CAP sensitivity of vagal afferent neurons, particularly when dealing with isolated neuron preparations.

Implications concerning ontogeny and action potential dynamics

A striking feature of the scatter plots of APFT, UV_{APD50} and DV_{APD50} measures from somatic action potentials of adult (n = 76) nodose neurons with intact axons as compared with identical measures of somatic action potential waveshape of isolated neonatal (n = 240, 3–9 day old) nodose neurons is the consistent statistical delineation ($p < 0.05$) of three populations of afferent

neurons. (Figures 2 and 3) Careful examination of the waveform measures presented in Table 1 reveal intriguing evidence of not only the dynamic differences across the three afferent populations but the potential for coordinated evolution of these differences with age. For example, we have previously shown that A-type nodose neurons express a single, tetrodotoxin-sensitive Na^+ current that underlies the rapid upstroke velocity of these myelinated afferents. (Schild, Clark et al., 1994) Furthermore, it has long been established that Na^+ expression at the soma increases with age and in cells expressing both tetrodotoxin-sensitive and tetrodotoxin-resistive Na^+ channels there occurs an age dependent change in the relative somatic expression of each Na^+ channel subtype.(Roy and Narahashi, 1992) However, even a substantial increase in Na^+ channel expression with age may not be expected to produce a significant increase in upstroke velocity because of the observed ~50% increase in WCC from neonatal to adult (i.e. $\frac{dV}{dt}=\frac{1}{WCC}\sum I_{Na} * \Delta t$). A functional characteristic that is evident across all three afferent types of neonatal and adult nodose neurons (Table 1). Interestingly, there was a marked increase in the downstroke velocity of A-type afferent neurons with a concomitant decrease in action potential duration. This would suggest a net increase in the total outward K^+ current well in excess of that needed to compensate for the increased ionic charge necessary to accommodate for the substantial increase in WCC. This most likely was a result of an increase in the fast inactivating 4-aminopyridine sensitive K^+ current which has been shown to parallel an increase in cell excitability in response to step current depolarization.(Schild, Clark et al., 1994) Surprisingly, such compensation was not observed in the other myelinated Ah-type or unmyelinated C-type cell types, both of which showed marked increase in APD_{50} with age.

While there was effectively no difference in resting membrane potential (RMP) across the three afferent populations nor between the two age groups there were clear differences in the thresholds for action potential discharge (APFT, Table 1). The pooled data showed statistically significant ($p < 0.05$ all populations) differences between the APFT of the three afferent populations with a trend toward more negative potentials at an increased age; i.e. APFT for (adult vs. neonatal) in A-type (−47.7 ± 2.0 vs. −43.3 ± 2.9), Ah-type (−41.0 ± 3.0 vs. −36.7 ± 2.7) and C-type (−32.8 ± 2.6 vs. −29.0 ± 3.3). This does not imply, however, an increased sensitivity to depolarizing currents because the concomitant increase in WCC would necessitate an increase in total charge to drive the membrane potential toward the lower APFT.

Collectively, such examples of ontogenic progression of neuronal characteristics may be a consequence of factors related to the physiological target of the sensory afferent termination. Further investigation of the underlying mechanisms for and the significance of these age dependent differences in somatic action potential characteristics are beyond the scope of this study. However, the robustness of the collective use of APFT, UV_{APD50}, and DV_{APD50} for segregation of isolated nodose neurons into three functionally distinct and statistically unique cell populations is evident in that afferent fiber type can be reliably identified across growth and development of the peripheral nervous system (Table 1, Figure 3).

Homogeneity of soma size across vagal afferents

The physical size of the neuronal soma quantified according to measures of cell diameter or corresponding whole cell capacitance (WCC) is an often used indicator of afferent fiber type. This has proven to be a convenient method for correlating classes of chemical activators of sensory neurons in the DRG with a presumption of afferentation.(Wood and Docherty, 1997) However, substantial evidence exists in the DRG literature that such indirect methods of anatomical classification are an oversimplification.(Harper and Lawson, 1985a;Harper and Lawson, 1985b; Lee, Chung et al., 1986;Villiere and McLachlan, 1996). Similar evidence exists for overlapping of soma diameters for visceral neurons with myelinated and

unmyelinated afferent fibers (Jaffe and Sampson, 1976;Gallego and Eyzaguirre, 1978) Throughout our experiments WCC was recorded and showed a normal distribution with no statistical difference noted across all populations of afferent fiber types and cell preparations (Table 1). The only exception to this being a somewhat expected increase (~30%) in WCC of adult nodose neurons as compared with neonatal cells. Therefore, these data suggest that the physical dimensions of nodose sensory neurons, either from an intact ganglia or isolated cell preparation should not be used as an indicator of afferent fiber type.

Conclusion

This study has made several contributions that will markedly advance our ability to interpret the functional significance of electrophysiological and chemophysiological properties of vagal sensory neurons enzymatically isolated from the nodose ganglion. First, in the rat nodose ganglia (Figure 1), as in rabbit(Stansfeld and Wallis, 1985), there exists a population of myelinated afferents with broad somatic action potential waveshapes that closely approximates that ubiquitously exhibited by vagal afferent neurons with unmyelinated afferent fibers. Furthermore, the prevalence of these Ah-type myelinated afferents (~12% of nodose neurons) is comparable to that of the population of A-type myelinated afferents with narrow (< 1 m/s) somatic action potential waveforms (~13% of nodose neurons). Second, while quantification of fiber conduction velocity remains the standard for functional classification of an afferent as myelinated or unmyelinated, collective measures of APFT, UV_{APD50} and DV_{APD50} of the patch evoked somatic action potential can be used as a reliable indicator of afferent fiber type (Figure 3). Third, for isolated cellular preparations that preclude the recording of an evoked action potential (e.g. voltage clamp protocols with intra- and extracellular recording solutions lacking K^+ ions, Figure 5) a differential sensitivity to the selective purinergic receptor (P2X) agonist αβ-m-ATP and the selective vanilloid receptor (VR1) agonist CAP can be used as reliable pharmacological indicators of afferent fiber type (Figures 4 and 5). Also, if voltage clamp protocols can be reliably carried out using an intact ganglion preparation (e.g. some K^+ channel currents, see(Li and Schild, 2002)) then a cell attached patch configuration can reliably quantify afferent fiber CV. (Figure 2)

When used in conjunction with patch clamp electrophysiological studies of isolated vagal sensory neurons, where transmembrane voltage, current and pharmacological challenges can be precisely measured and controlled, these validated correlates of afferent fiber type can be used to provide valuable insight concerning the relavence of isolated cellular observations to the neurophysiological afferent function of intact visceral organ systems.

Acknowledgements

This work was supported by award HL072012 from the National Institute of Health.

Reference List

Bailey TW, Jin YH, Doyle MW, Andresen MC. Vanilloid-sensitive afferents activate neurons with prominent A-type potassium currents in nucleus tractus solitarius. J Neurosci 2002;22:8230–7. [PubMed: 12223577]

Belmonte C, Gallego R. Membrane properties of cat sensory neurones with chemoreceptor and baroreceptor endings. J Physiol (Lond) 1983;342:603–14. [PubMed: 6631751]

Benson CJ, Eckert SP, McCleskey EW. Acid-evoked currents in cardiac sensory neurons: A possible mediator of myocardial ischemic sensation. Circ Res 1999;84:921–8. [PubMed: 10222339]

Bielefeldt K. Differential effects of capsaicin on rat visceral sensory neurons. Neuroscience 2000;101:727–36. [PubMed: 11113321]

Blackshaw LA, Brookes SJ, Grundy D, Schemann M. Sensory transmission in the gastrointestinal tract. Neurogastroenterol Motil 2007;19:1–19. [PubMed: 17280582]

Cabanes C, Lopez dA, Viana F, Belmonte C. Postnatal changes in membrane properties of mice trigeminal ganglion neurons. Journal of Neurophysiology 2002;87:2398–407. [PubMed: 11976377]

Clapham DE. TRP channels as cellular sensors. Nature 2003;426:517–24. [PubMed: 14654832]

Doyle MW, Bailey TW, Jin YH, Andresen MC. Vanilloid receptors presynaptically modulate cranial visceral afferent synaptic transmission in nucleus tractus solitarius. J Neurosci 2002;22:8222–9. [PubMed: 12223576]

Dunn PM, Zhong Y, Burnstock G. P2X receptors in peripheral neurons. Progress in Neurobiology 2001;65:107–34. [PubMed: 11403876][Review] [223 refs]

Fan W, Andresen MC. Differential frequency-dependent reflex integration of myelinated and nonmyelinated rat aortic baroreceptors. Am J Physiol 1998;275:H632–H640. [PubMed: 9683453]

Fan W, Schild JH, Andresen MC. Graded and dynamic reflex summation of myelinated and unmyelinated rat aortic baroreceptors. Am J Physiol 1999;277:R748–R756. [PubMed: 10484492]

Gallego R, Eyzaguirre C. Membrane and action potential characteristics of A and C nodose ganglion cells studied in whole ganglia and in tissue slices. J Neurophysiol 1978;41:1217–32. [PubMed: 702193]

Glazebrook PA, Schilling WP, Kunze DL. TRPC channels as signal transducers. Pflugers Arch 2005;451:125–30. [PubMed: 15971079]

Gorelik J, Gu Y, Spohr HA, Shevchuk AI, Lab MJ, Harding SE, Edwards CR, Whitaker M, Moss GW, Benton DC, Sanchez D, Darszon A, Vodyanoy I, Klenerman D, Korchev YE. Ion channels in small cells and subcellular structures can be studied with a smart patch-clamp system. Biophys J 2002;83:3296–303. [PubMed: 12496097]

Harper AA, Lawson SN. Conduction velocity is related to morphological cell type in rat dorsal root ganglion neurones. J Physiol (Lond) 1985a;359:31–46. [PubMed: 3999040]

Harper AA, Lawson SN. Electrical properties of rat dorsal root ganglion neurones with different peripheral nerve conduction velocities. J Physiol (Lond) 1985b;359:47–63. [PubMed: 2987489]

Hjerling-Leffler J, Alqatari M, Ernfors P, Koltzenburg M. Emergence of functional sensory subtypes as defined by transient receptor potential channel expression. J Neurosci 2007;27:2435–43. [PubMed: 17344381]

Huang TY, Hanani M. Morphological and electrophysiological changes in mouse dorsal root ganglia after partial colonic obstruction. Am J Physiol Gastrointest Liver Physiol 2005;289:G670–G678. [PubMed: 15920014]

Jaffe RA, Sampson SR. Analysis of passive and active electrophysiologic properties of neurons in mammalian nodose ganglia maintained in vitro. J Neurophysiol 1976;39:802–15. [PubMed: 9491]

Jin YH, Bailey TW, Li BY, Schild JH, Andresen MC. Purinergic and vanilloid receptor activation releases glutamate from separate cranial afferent terminals in nucleus tractus solitarius. J Neurosci 2004;24:4709–17. [PubMed: 15152030]

Kobayashi K, Fukuoka T, Obata K, Yamanaka H, Dai Y, Tokunaga A, Noguchi K. Distinct expression of TRPM8, TRPA1, and TRPV1 mRNAs in rat primary afferent neurons with adelta/c-fibers and colocalization with trk receptors. J Comp Neurol 2005;493:596–606. [PubMed: 16304633]

Kollarik M, Dinh QT, Fischer A, Undem BJ. Capsaicin-sensitive and -insensitive vagal bronchopulmonary C-fibres in the mouse. J Physiol 2003;551:869–79. [PubMed: 12909686]

Kubin L, Alheid GF, Zuperku EJ, McCrimmon DR. Central pathways of pulmonary and lower airway vagal afferents. J Appl Physiol 2006;101:618–27. [PubMed: 16645192]

Lancaster E, Weinreich D. Sodium currents in vagotomized primary afferent neurones of the rat. J Physiol 2001;536:445–58. [PubMed: 11600680]

Lee KH, Chung K, Chung JM, Coggeshall RE. Correlation of cell body size, axon size, and signal conduction velocity for individually labelled dorsal root ganglion cells in the cat. J Comp Neurol 1986;243:335–46. [PubMed: 3950079]

Li BY, Schild JH. Patch clamp electrophysiology in nodose ganglia of adult rat. Journal of Neuroscience Methods 2002;115:157–67. [PubMed: 11992667]

Mei N, Condamin M, Boyer A. The composition of the vagus nerve of the cat. Cell Tissue Res 1980;209:423–31. [PubMed: 7407841]

Roy ML, Narahashi T. Differential properties of tetrodotoxin-sensitive and tetrodotoxin- resistant sodium channels in rat dorsal root ganglion neurons. J Neurosci 1992;12:2104–11. [PubMed: 1318956]

Ruscheweyh R, Forsthuber L, Schoffnegger D, Sandkuhler J. Modification of classical neurochemical markers in identified primary afferent neurons with Abeta-, Adelta-, and C-fibers after chronic constriction injury in mice. J Comp Neurol 2007;502:325–36. [PubMed: 17348016]

Santiago S, Ferrer T, Espinosa ML. Neurophysiological studies of thin myelinated (A delta) and unmyelinated (C) fibers: application to peripheral neuropathies. Neurophysiol Clin 2000;30:27–42. [PubMed: 10740794]

Schild JH, Clark JW, Hay M, Mendelowitz D, Andresen MC, Kunze DL. A- and C-type rat nodose sensory neurons: model interpretations of dynamic discharge characteristics. J Neurophysiol 1994;71:2338–58. [PubMed: 7523613]

Schild JH, Kunze DL. Experimental and modeling study of Na+ current heterogeneity in rat nodose neurons and its impact on neuronal discharge. J Neurophysiol 1997;78:3198–209. [PubMed: 9405539]

Seagard JL, Hopp FA, Drummond HA, Van Wynsberghe DM. Selective contribution of two types of carotid sinus baroreceptors to the control of blood pressure. Circ Res 1993;72:1011–22. [PubMed: 8477517]

Stansfeld CE, Wallis DI. Properties of visceral primary afferent neurons in the nodose ganglion of the rabbit. J Neurophysiol 1985;54:245–60. [PubMed: 4031986]

Stett A, Burkhardt C, Weber U, van SP, Knott T. CYTOCENTERING: a novel technique enabling automated cell-by-cell patch clamping with the CYTOPATCH chip. Receptors Channels 2003;9:59–66. [PubMed: 12825299]

Sugiura T, Dang K, Lamb K, Bielefeldt K, Gebhart GF. Acid-sensing properties in rat gastric sensory neurons from normal and ulcerated stomach. J Neurosci 2005;25:2617–27. [PubMed: 15758172]

Villiere V, McLachlan EM. Electrophysiological properties of neurons in intact rat dorsal root ganglia classified by conduction velocity and action potential duration. Journal of Neurophysiology 1996;76:1924–41. [PubMed: 8890304]

Wang X, Li M. Automated electrophysiology: high throughput of art. Assay Drug Dev Technol 2003;1:695–708. [PubMed: 15090242]

Waxman SG. Acquired channelopathies in nerve injury and MS. Neurology 2001;56:1621–7. [PubMed: 11428390][Review] [62 refs]

Wood JN, Docherty R. Chemical activators of sensory neurons. Annu Rev Physiol 1997;59:457–82. [PubMed: 9074773]

Yoshida S, Matsumoto S. Effects of alpha-dendrotoxin on K+ currents and action potentials in tetrodotoxin-resistant adult rat trigeminal ganglion neurons. J Pharmacol Exp Ther 2005;314:437–45. [PubMed: 15831438]

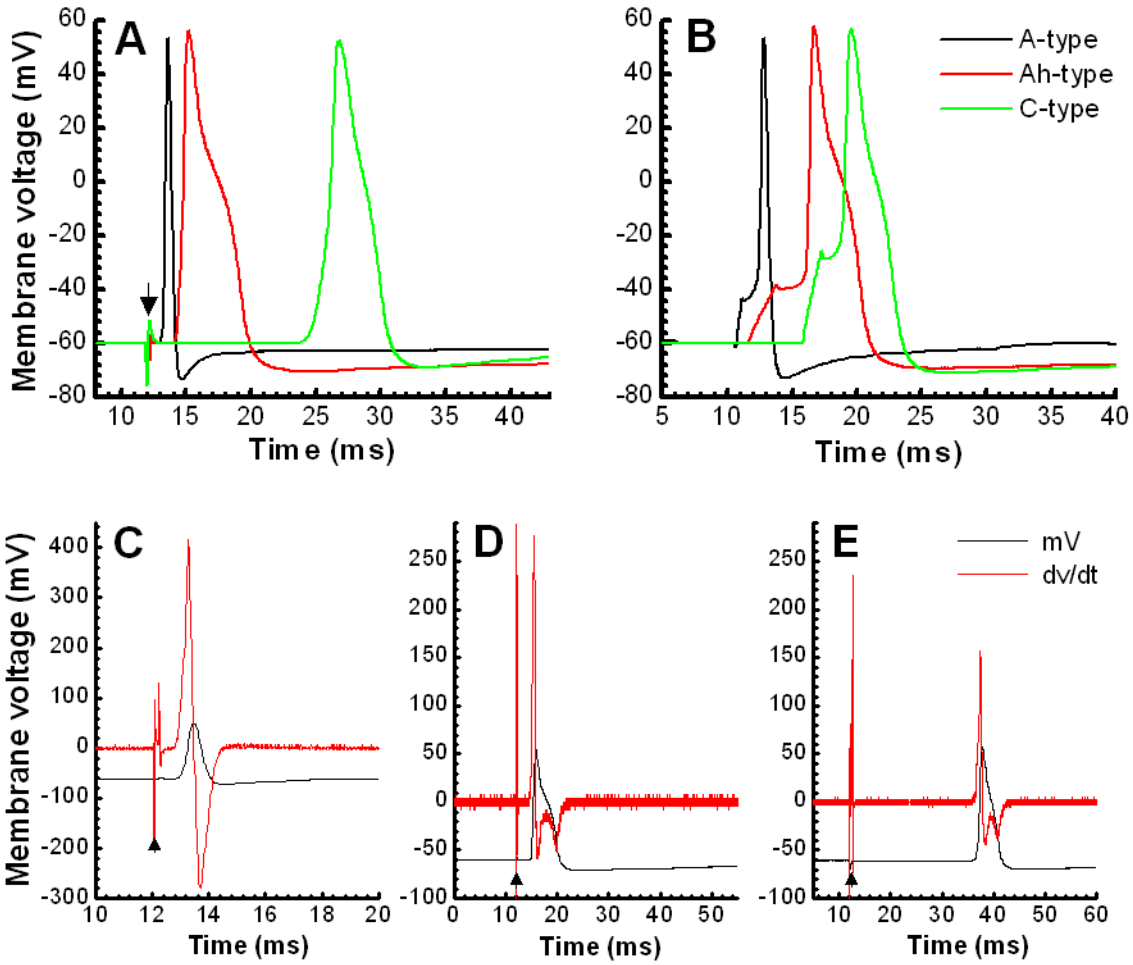

Figure 1. Validation of cell-type and CV measures using the cell attached technique

Somatic APs elicited by vagal (**A**) and soma (**B**) stimulation from the same A-, Ah, and C-type NGNs, respectively.

The calculations of CVs from currents obtained from cell-attached recording (*upper panel*) under the voltage-clamp mode (**C**, **D**, and **E**) closely match those from whole-cell current-clamp recordings (*lower panel*). CVs are 14.76 m/s for A-type, 10.59 m/s for Ah-type, and 0.79 m/s for C-type, respectively. The 2nd peak (*) of current obtained from cell-attached recording represents the repolarization hump seen at the AP of Ah- and C-type NGNs only. Dark filled triangles represent the stimulus artifacts.

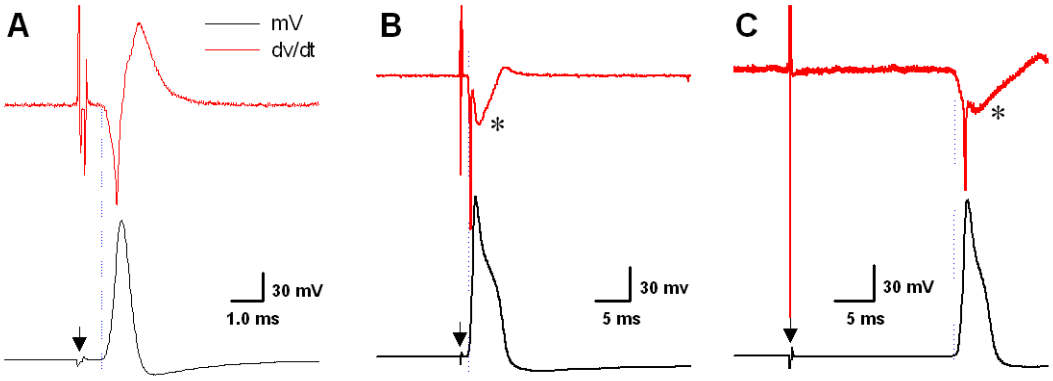

Figure 2. Validation of upstroke velocity as an indicator of afferent fiber type

Nerve-evoked somatic action potentials from nodose neurons in an intact ganglia (dark traces) and corresponding time derivative (gray traces). (**A**) A-type, myelinated afferent. (**B**) Ah-type, myelinated afferent. (**C**) C-type, unmyelinated afferent. Filled triangles demarcate artifact from nerve stimulation. Asterisk (*) highlights the marked effect of the “hump” or delay in repolarization has upon the time derivative measure of downstroke velocity.

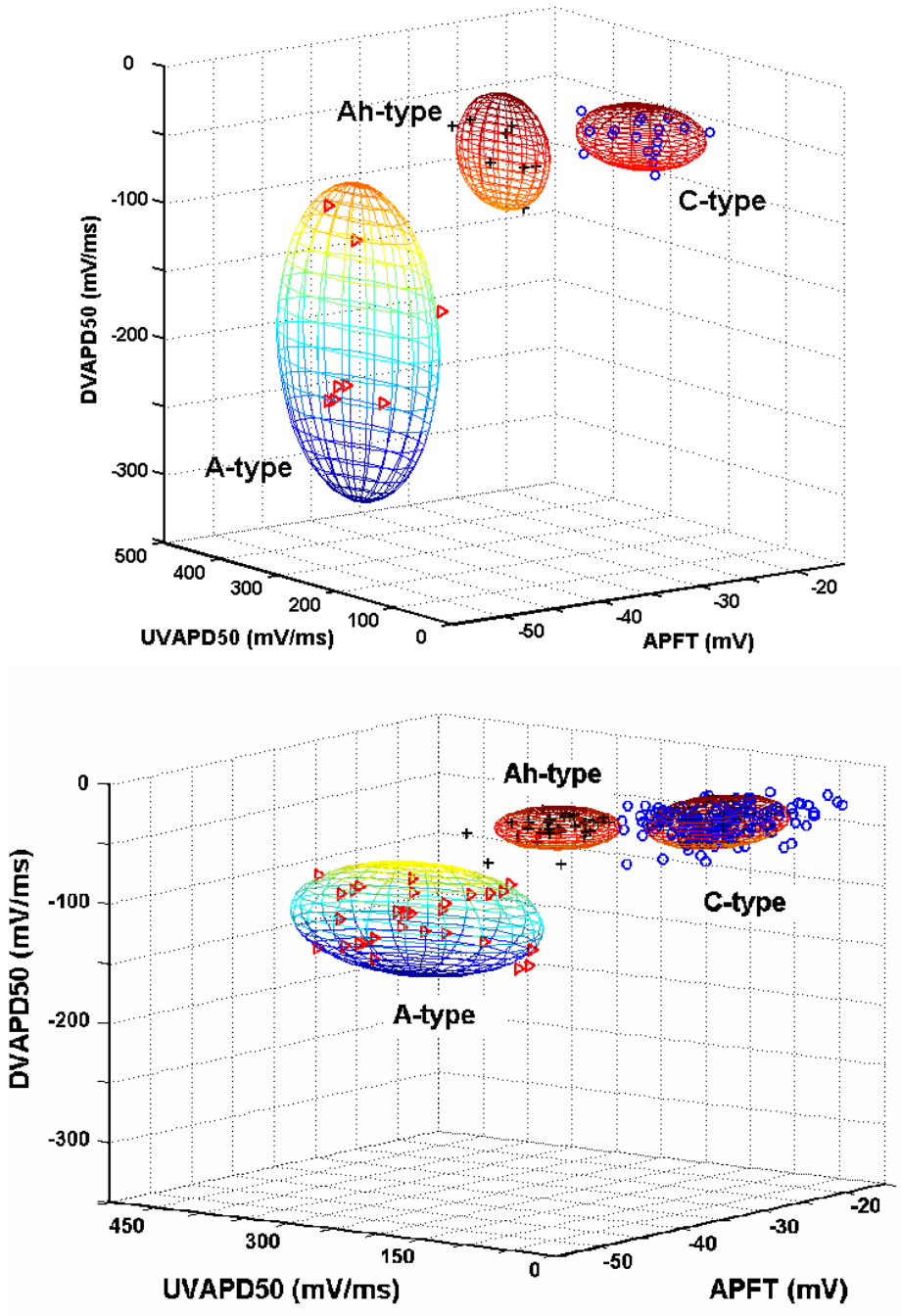

Figure 3. Classification of afferent fiber type based upon collective waveshape measures

Clustering of APFT, UV_{APD50}, and DV_{APD50} can segregate somatic action potential waveforms according to afferent fiber type. Each sphere demarcates two standard deviations from the mean ($P < 0.05$). **Upper-panel**: Measures from somatic action potentials from intact ganglion were fiber type can be validated according to CV. **Bottom panel**: Clustering of measures from somatic action potentials from isolated neonatal nodose neurons (n = 240). In all panels, the triangles, crosses and circles represent A-, Ah- and C-type nodose neurons, respectively.

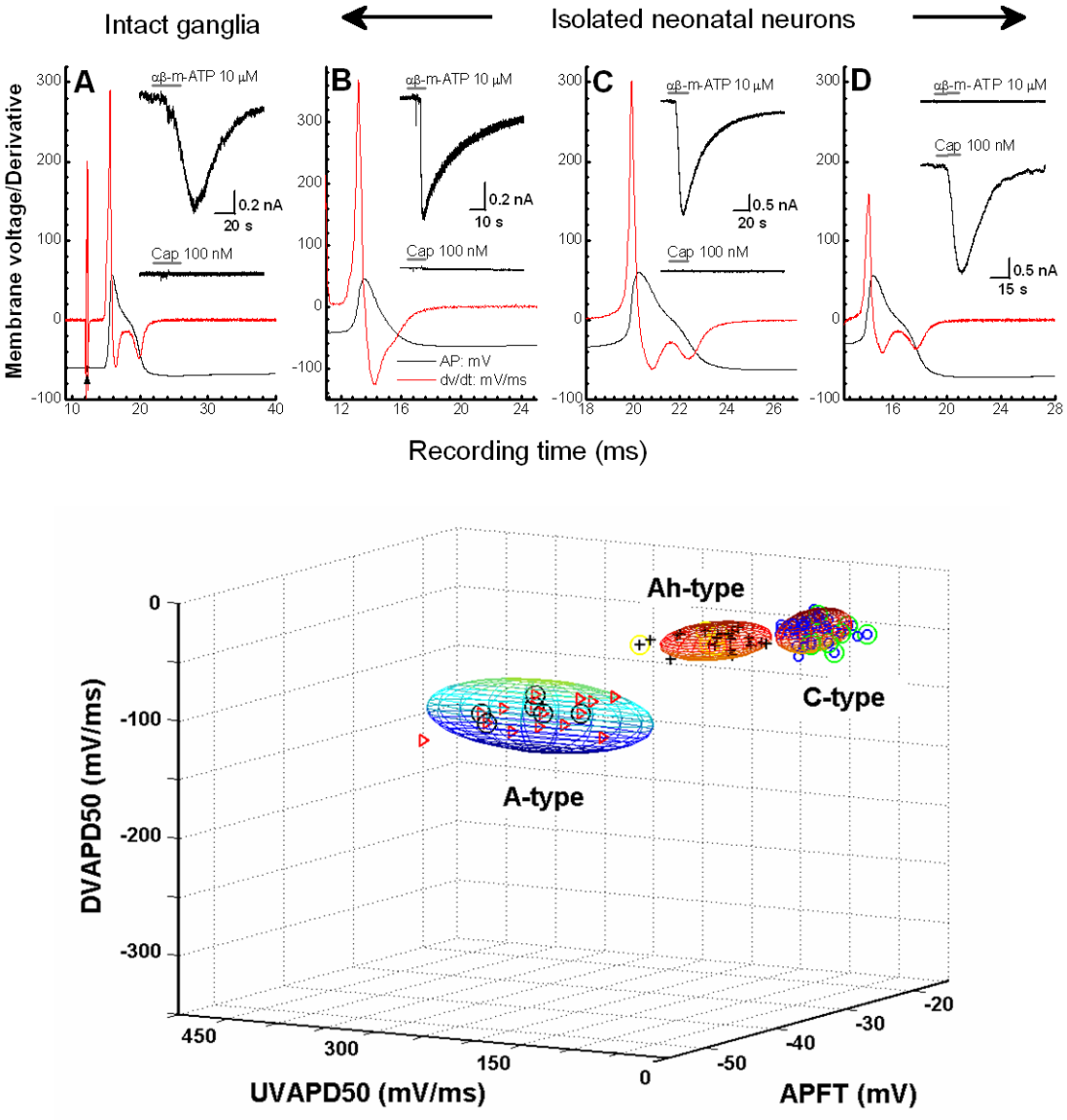

Figure 4. Validation of pharmacological classification

A) Nerve evoked action potential of an Ah-type nodose neuron as identified by CV, UV_{APD50}, DV_{APD50} and the presence of delayed repolarization. **B – D)** Isolated A-, Ah-, and C-type neonatal nodose neurons classified according to UV_{APD50}, DV_{APD50} and the absence or presence of delayed repolarization and differential sensitivity to agonist challenges of 10 μM αβ-m-ATP (*insets top trace*) and 100 nM CAP (*insets bottom traces*). **Lower-panel:** Clustering of measures from somatic action potentials from isolated neonatal nodose neurons (n = 74) where only those identified as C-type exhibited a positive response to 100 nM CAP. In all panels, the triangles, crosses and circles represent A-, Ah- and C-type nodose neurons, respectively. All sample points with circles represent cells challenged with both 10 μM αβ-m-ATP and 100 nM CAP: Triangle w/circle are αβ-m-ATP-positive and CAP-negative A-type neurons without a repolarization hump; Cross w/circle are αβ-m-ATP-positive and CAP-negative neurons with a repolarization hump are Ah-type neurons; Circles w/in circles are αβ-m-ATP-negative and CAP-positive neurons with a repolarization hump are C-type neurons.

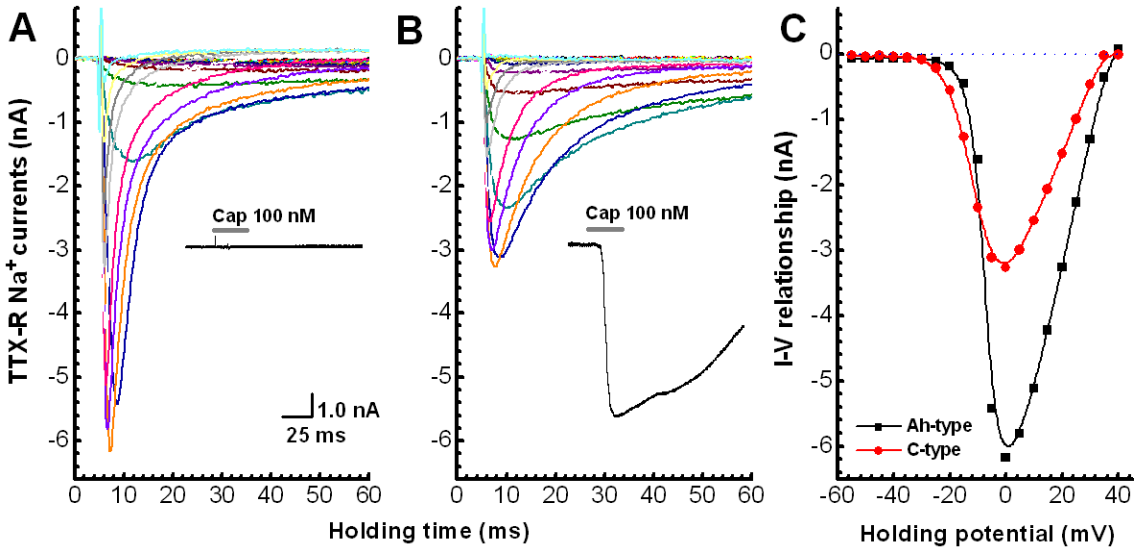

Figure 5. Pharmacological classification of cell type and whole cell Na^+ current

Neurons enzymatically isolated from adult ganglia and prepared for voltage clamp recording of whole cell Na^+ currents (see Methods). Cell type classified as either Ah- or C-type based upon a differential sensitivity to TTX (1.0 μM) and CAP (100 nM). **A)** *Ah-type*: cell was unresponsive to CAP and exhibited a large inward Na^+ current resistant to TTX. **B)** *C-type*: cell exhibited a large inward current in the presence of CAP and also exhibited an inward Na^+ current resistant to TTX although with somewhat different voltage- and time-dependent characteristics. Insets in **(A)** and **(B)** are whole cell current response to application of 100 nM CAP. **C)** comparison of current-voltage (IV) relationship of the peak inward TTX-resistant Na^+ current from Ah- and C-type neurons.

Table 1

Measures of AP waveshape characteristics

Columns under the heading of **Intact ganglia** are measures from nodose neurons within an intact adult ganglia and with afferent classification based upon measure of CV (A-type: n = 10, Ah-type: n = 9, and C-type: n = 57). Columns under the heading of **Isolated** are measures from enzymatically isolated neonatal nodose neurons with afferent classification based upon measures of action potential waveshape (A-type: n = 29, Ah-type: n = 27, and C-type: n = 184). All somatic action potentials evoked by current injection through the patch electrode (see Figure 1B). Data presented as mean ± SD. *P < 0.05 and **P < 0.01 vs. A-type, $^{\#\#}$P < 0.01 vs. C-type.

Parameter	ANOVA 0.05/0.01	Intact ganglia A-type	Intact ganglia Ah-type	Intact ganglia C-type	ANOVA 0.05/0.01	Isolated A-type	Isolated Ah-type	Isolated C-type
CV	Y/Y	14.0 ± 1.0	10.5 ± 4.4 $^{\#\#}$	0.68 ± 0.1	NA	NA	NA	NA
RMP	N/N	−62 ± 4	−63.5 ± 2.5	−65 ± 5	N/N	−62 ± 3.4	−64 ± 3.2	−64 ± 4.4
APFT	Y/Y	−47.7 ± 2.0	−41 ± 3 **$^{/\#\#}$	−32.8 ± 2.6	Y/Y	−43.3 ± 2.9	−36.7 ± 2.7 **$^{/\#\#}$	−29 ± 3.3
APD_{50}	Y/Y	0.78 ± 0.12	2.3 ± 0.8 **	3.1 ± 1.0	Y/Y	0.84 ± 0.14	1.86 ± 0.4 **	2.57 ± 0.8
$Peak_{AP}$	N/N	47.4 ± 5.6	46.6 ± 7.7	50 ± 8	N/N	46 ± 5.3	56 ± 2.9	49 ± 5.4
AHP_{80}	Y/Y	9.0 ± 5.58	58 ± 34 **	44 ± 24	Y/Y	23 ± 13	50 ± 28 *	66 ± 23
$Peak_{AHP}$	N/N	−68.4 ± 2.9	−67 ± 3	−64 ± 18	N/N	−66.9 ± 2.3	−65.6 ± 2.4	−68 ± 3.4
UV_{APD50}	Y/Y	287 ± 76	195 ± 53 **$^{/\#\#}$	83 ± 42	Y/Y	267 ± 66	168 ± 29.1 $^{\#\#}$	64 ± 29
DV_{APD50}	Y/Y	−160 ± 54	−32 ± 13 **	−31 ± 12	Y/Y	−110 ± 27	−35.7 ± 13 **	−31.5 ± 9.9
UV_{MAX}	Y/Y	383 ± 75	251 ± 52 **$^{/\#\#}$	140 ± 56	Y/Y	372 ± 82	305 ± 34 *$^{/\#\#}$	164 ± 45
DV_{MAX}	Y/Y	−184 ± 62	−61 ± 17 **	−50 ± 14	Y/Y	−142. ± 26	−69.5 ± 17 **	−55 ± 12
WCC	N/N	48.8 ± 5.63	47.9 ± 5.38	48.5 ± 7.37	N/N	32.6 ± 6.67	32.2 ± 6.41	31.8 ± 5.70

Note: **CV** (m/s): Conduction velocity; **RMP** (mV): Resting membrane potential. **APFT** (mV): AP firing threshold measured from APs evoked by soma stimulation; **APD_{50}** (ms): Action potential duration at the point of 50% height of AP. **$Peak_{AP}$** (mV): Peak of AP. **AHP_{80}** (ms): The time of 80% recovery of after hyperpolarization. **$Peak_{AHP}$** (mV): Peak of after hyperpolarization. **UV_{APD50}** (mV/ms): Upstroke velocity at the point of APD_{50}. **DV_{APD50}** (mV/ms): Downstroke velocity at the point of APD_{50}. **UV_{MAX}** (mV/ms): Maximal upstroke velocity. **DV_{MAX}** (mV/ms): Maximal downstroke velocity. **WCC**: whole-cell capacitance (pF).